JOURNAL OF MATERIALS SCIENCE 15 (1980) 3150–3156

Plastic deformation mechanisms in tungsten carbide

J. D. BOLTON, M. REDINGTON
The National Institute for Higher Education, Limerick, Ireland

Transmission electron microscopy studies of dislocations formed by plastic deformation in tungsten carbide have confirmed a slip deformation mechanism involving the $\{1\,0\,\bar{1}\,0\}\langle 0\,0\,0\,1\rangle$ system. Direct visual evidence also confirmed the existence of extended dislocations formed by a suggested dissociation $1/3\langle 1\,1\,\bar{2}\,3\rangle = 1/6\langle 2\,0\,\bar{2}\,3\rangle + 1/6\langle 0\,2\,\bar{2}\,3\rangle$ which can further interact with other extended dislocations on pairs of intersecting $\{1\,1\,\bar{2}\,2\}$ pyramidal planes. The proposed interaction is suggested as a means of reducing both dislocation strain energy and atomic misfit strains due to antiphase boundary formation and leads to a form of sessile dislocation arrangement similar to the Lomer Cottrell lock.

1. Introduction

The aim of this article is to report some observations made during the study of dislocations in plastically deformed tungsten carbide.

Refractory tungsten carbide forms an important component of wear and abrasion resistant materials which are normally prepared as sintered aggregates involving cobalt as a binding phase. Until relatively recently the ability of these sintered hardmetals to undergo plastic deformation has been attributed totally to plastic deformation in the soft cobalt binder phase, but evidence now exists [1–6] for slip deformation within the tungsten carbide itself, especially in low cobalt grade materials.

In this particular experimental work we have attempted to identify some of the dislocation mechanisms for slip in tungsten carbide by transmission electron microscopy (TEM) and have succeeded in providing some new and alternative ideas to previous work as well as giving confirmation to some existing ideas.

2. Background crystallographic features of tungsten carbide

The hexagonal structure of tungsten carbide contrasts with the close-packed hexagonal metal structures in that it has a low c/a ratio i.e. 0.97, extreme anisotropy and an atomic packing sequence which essentially corresponds to an ordered lattice. This ordered arrangement consists of alternate tungsten and carbon layers in an ABAB packing sequence with the B layer of small carbon atoms being responsible for the very low c/a ratio. As a consequence of these two effects, plastic deformation mechanisms in tungsten carbide may not reproduce those found in the more typical hexagonal metals, and electron

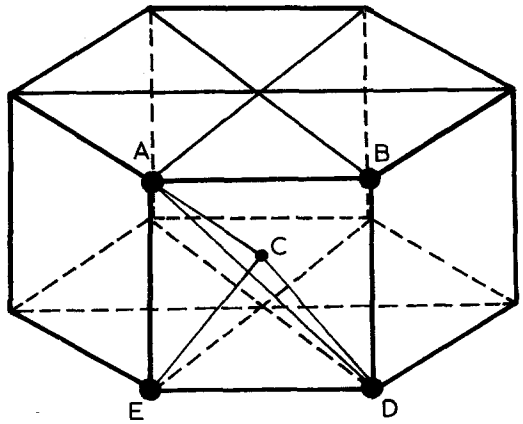

Figure 1 Position C corresponds to the carbon atom site in the B layer, positions ABED correspond to tungsten atoms in the A layer. *Slip Vectors*: BD = $\langle 0\,0\,0\,1\rangle$, Plane $\{1\,0\,\bar{1}\,0\}$; AD = $\frac{1}{3}\langle 1\,1\,\bar{2}\,3\rangle$, Plane $\{1\,0\,\bar{1}\,0\}$ or $\{1\,1\,\bar{2}\,2\}$; AB = $\frac{1}{3}\langle 2\,\bar{1}\,\bar{1}\,0\rangle$, Plane $\{0\,0\,0\,1\}$ or $\{1\,0\,\bar{1}\,0\}$; EC, DC and CA = $\frac{1}{6}\langle 2\,0\,\bar{2}\,3\rangle$, Plane $\{1\,1\,\bar{2}\,2\}$. *Combined Vectors*: AD = AB + BD; AD = DC + CA; AE = AC + CE and AB = EC + CD.

0022–2461/80/123150–07$02.70/0

diffraction conditions can alter from the expected h c p mode.

Suggested and observed slip systems for tungsten carbide involve prismatic and pyramidal slip planes, but do not include basal slip despite the fact that this plane has a high packing density. A possible explanation for the apparent absence of basal slip is that extremely strong interatomic bond forces exist between carbon and tungsten atoms across the ABAB layers which prevent shearing along directions in the basal plane. Potential prismatic and pyramidal slip systems are shown in Fig. 1 and also in a stereographic projection mode in Fig. 2. These systems can be summarized as follows.

2.1. Prismatic slip

The following unit dislocations on the $\{1\,0\,\bar{1}\,0\}$ planes are possible.

(1) Burger's vector, $\mathbf{b} = \langle 0\,0\,0\,1\rangle$;
Energy ($\propto \mathbf{b}^2$) $= 0.94a^2$

(2) Burger's vector, $\mathbf{b} = \frac{1}{3}\langle 1\,1\,\bar{2}\,3\rangle$;
Energy ($\propto \mathbf{b}^2$) $= 1.94a^2$

(3) Burger's vector, $\mathbf{b} = \frac{1}{3}\langle 2\,\bar{1}\,\bar{1}\,0\rangle$;
Energy ($\propto \mathbf{b}^2$) $= 1a^2$

Unit dislocations of the type $\mathbf{b} = \langle 0\,0\,0\,1\rangle$ also have the potential for dissociation on $\{\bar{1}\,2\,\bar{1}\,0\}$ prism planes into partials of the type $\langle 0\,0\,0\,1\rangle \rightarrow 1/6\langle\bar{2}\,0\,2\,3\rangle + 1/6\langle 2\,0\,\bar{2}\,3\rangle$ but such a reaction would involve a slight energy increase, $0.94a^2 \rightarrow (0.57a^2 + 0.57a^2)$.

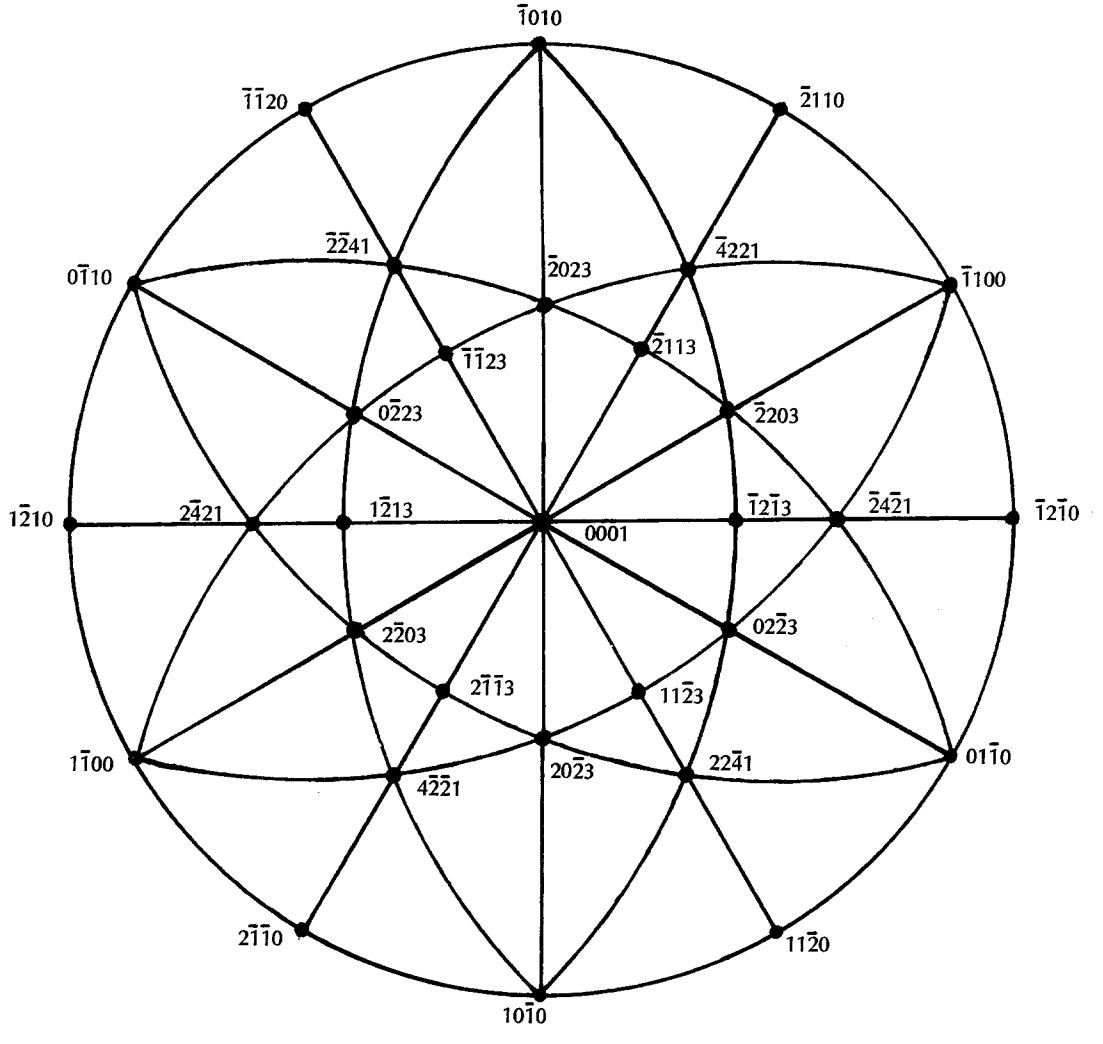

Figure 2 Standard [0 0 0 1] projection for tungsten carbide c/a ratio 0.97 including $\{1\,0\,\bar{1}\,0\}$ prism, $\{1\,1\,\bar{2}\,2\}$ pyramidal slip planes and potential Burgers vectors.

2.2. Pyramidal planes

The following dislocation on the $\{2\bar{1}\bar{1}2\}$ planes is possible.

Burger's vector, $\mathbf{b} = \frac{1}{3}\langle\bar{2}113\rangle$.

This dislocation also has the potential for dissociation according to the reaction, $1/3\langle\bar{2}113\rangle = 1/6\langle\bar{2}023\rangle + 1/6\langle\bar{2}203\rangle$ and is favoured by an energy decrease from $1.94a^2$ to $(0.57a^2 + 0.57a^2)$. Unit dislocations of the type $1/3\langle\bar{2}113\rangle$ also have the further possibility of cross slip into both $\{10\bar{1}0\}$ prism and $\{1\bar{2}11\}/\{10\bar{1}1\}$ pyramidal planes, see Fig. 2. Of particular interest in this note is the potential existence of partial dislocations of the type $1/6\langle20\bar{2}3\rangle$ which not only create stacking faults but also lead to the formation of antiphase boundaries by displacing tungsten atoms into carbon atom positions in the ordered structure.

3. Analysis of TEM images

Specimen preparation involved the use of ion beam thinning of a thin slice taken at the fracture surface of a 9% cobalt transverse rupture specimen, and observations were made using a JEOL 100C microscope at 100 kV.

Standard analytical methods for imaging dislocations can be inapplicable to tungsten carbide due to the following reasons. (i) Lack of beam penetration, due to high density, limits the degree of foil tilting, and severely restricts the ability to obtain bright-field two-beam conditions. (ii) Inferred knowledge of crystal growth characteristics in tungsten carbide suggests that it is strongly anisotropic and, without knowledge of its anisotropic elastic properties, computer matching of dislocation images is unreliable. (iii) Differing atomic radii of the two atomic species within the crystal lattice cause major difficulties in calculating extinction distances.

Because of these problems alternative techniques for analysing dislocation images were adopted and relied either upon centred dark-field imaging of a dislocation or upon a simple geometric analysis of orientation relationships.

4. Results and Discussion

By constructing the image of a dislocation from a selected diffraction spot using the central dark field technique it can be argued that similar images produced from different diffraction spots obey the condition that $\mathbf{g}_1 \cdot \mathbf{b} = \mathbf{g}_2 \cdot \mathbf{b}$, where $\mathbf{b}$ is the Burgers vector and $\mathbf{g}_1$, $\mathbf{g}_2$ is the particular diffraction vectors which cause identical images.

Illustrative of this approach are the images shown in Fig. 3a to h where the bowed dislocation is viewed with $\{0001\}$ as the plane of the foil. Matching images of this dislocation occurred with centred dark field on the following pairs of diffraction spots. Fig. 3c and d on $\{1\bar{2}10\}$ and $\{\bar{1}2\bar{1}0\}$. Fig. 3e and f on $\{\bar{1}010\}$ and $\{10\bar{1}0\}$. Fig. 3g and h on $\{2\bar{3}10\}$ and $\{2\bar{4}20\}$. With the first of these matching pairs, extinction of the dislocation infers that $\mathbf{g}_1\mathbf{b}\cos\theta_1 = \mathbf{g}_2\mathbf{b}\cos\theta_2 = 0$ and since $\mathbf{g}_1 = -\mathbf{g}_2$, $\theta_1 = \theta_2 = 90°$. Possible solutions for $\mathbf{b}$, the Burgers vector, include any vector lying on the great circle $[\bar{1}010]$ $[0001]$ $[10\bar{1}0]$. θ_1 and θ_2 must also be equal for the second pair for the same reason that $\mathbf{g}_1 = -\mathbf{g}_2$ and $\mathbf{b}$ the Burgers vector can lie on any great circle passing through $[0001]$. In the third pair of like images, $\mathbf{g}_1$ and $\mathbf{g}_2$ are not equal so that only solutions giving $\mathbf{g}\cdot\mathbf{b} = 0$ can apply. This again infers that θ the angle between $\mathbf{g}$ and $\mathbf{b}$ must equal 90° and that $[0001]$ is the solution for $\mathbf{b}$. The common solution for the Burgers vector from all three pairs of matching images consists of the $[0001]$ direction and when also included with vectors defining the dislocation line suggests that $\{10\bar{1}0\}$ planes are the operative slip planes, in agreement with previous observations.

An alternative dislocation structure to that discussed above was also observed in the form of straight dislocation segments forming a parallelogram and is shown in Fig. 4. In this case extinction fringes plus streaking of the diffraction pattern suggest the existence of extended dislocations and the presence of stacking faults, which in relation to tungsten carbide should be more correctly termed as antiphase boundaries. Analysis of this dislocation carried out by single surface trace analysis led to the following conclusions. The parallelogram shaped dislocation array showed equi-spaced fringes on all sides after tilting the foil to bring a $\{10\bar{1}1\}$ plane normal parallel to the beam, and was oriented such that $(\bar{1}101)$ and $(\bar{1}011)$ plane normals lay parallel to the long and short parallelogram axes respectively. These orientation relationships plus the angular measurements between sides of the parallelogram strongly suggest that the parallelogram edges correspond to a pair of intersecting $\{11\bar{2}2\}$ planes which could for example be composed of a $(2\bar{1}\bar{1}2)$ plane along the long axis intersecting a $(\bar{1}2\bar{1}2)$ plane on the short axis. On each of these two intersecting

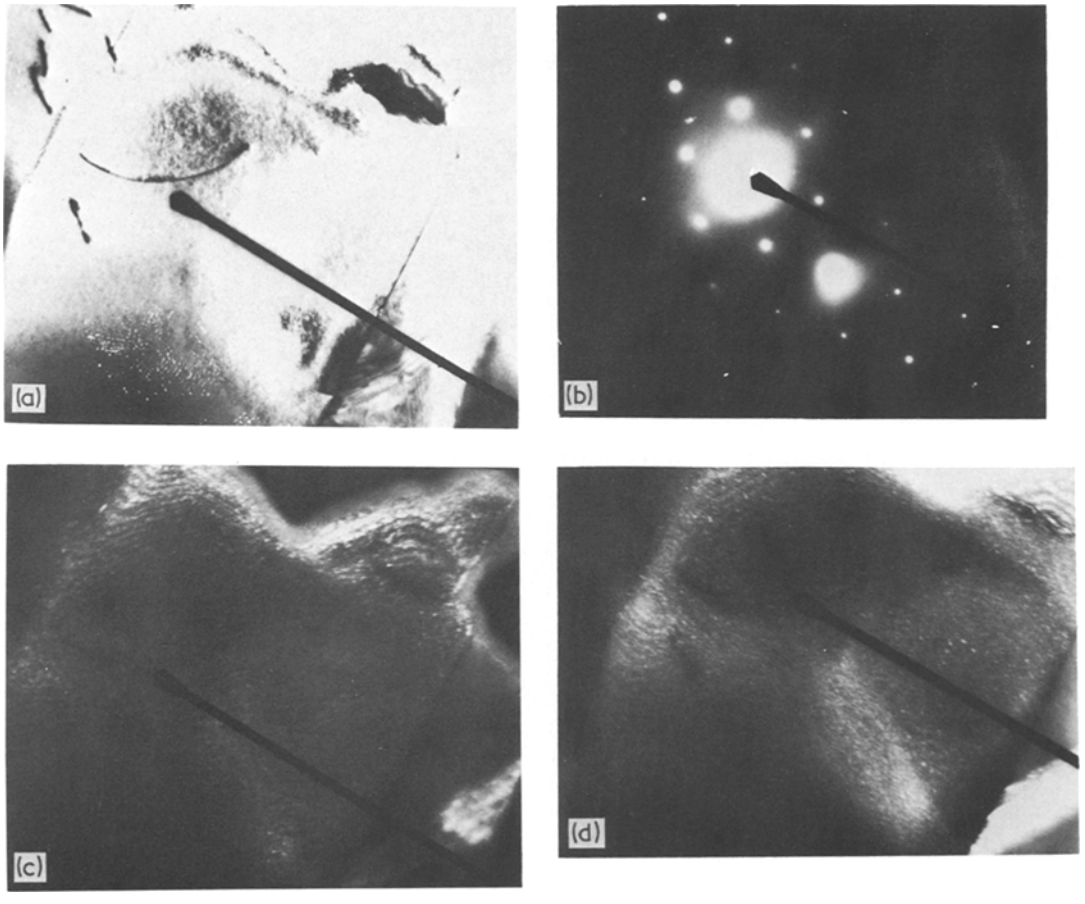

Figure 3 (a) Bright field (× 70 000). (b) $\{0\,0\,0\,1\}$ selected area diffraction pattern. (c) Dark field $\mathbf{g} = (1\,\bar{2}\,1\,0)$. (d) Dark field $\mathbf{g} = (\bar{1}\,2\,\bar{1}\,0)$. (e) Dark field $\mathbf{g} = (1\,0\,\bar{1}\,0)$. (f) Dark field $\mathbf{g} = (\bar{1}\,0\,1\,0)$. (g) Dark field $\mathbf{g} = (2\,\bar{3}\,1\,0)$. (h) Dark field $\mathbf{g} = (2\,\bar{4}\,2\,0)$.

pyramidal planes dissociation of unit dislocations into partials is possible according to the following reactions, see Fig. 2.

On $(2\,\bar{1}\,\bar{1}\,2)$ *plane*

$$\tfrac{1}{3}[\bar{2}\,1\,1\,3] \rightarrow \tfrac{1}{6}[\bar{2}\,0\,2\,3] + \tfrac{1}{6}[\bar{2}\,2\,0\,3]. \quad (1)$$

On $(\bar{1}\,2\,1\,\bar{2})$ *plane*

$$\tfrac{1}{3}[1\,\bar{2}\,1\,3] \rightarrow \tfrac{1}{6}[0\,\bar{2}\,2\,3] + \tfrac{1}{6}[2\,\bar{2}\,0\,3]. \quad (2)$$

Collision between the leading partials of these extended dislocations at plane intersections can lead to new dislocations being formed, and two particular reactions are significant in terms of the dislocation array shown by Fig. 4. Firstly, a possible reduction in strain energy can occur through the reaction $1/6[\bar{2}\,2\,0\,3] + 1/6[2\,\bar{2}\,0\,3] \rightarrow [0\,0\,0\,1]$ if the two trailing partials of the above reactions interact. A second possible reaction which involves an energy increase can occur between the two leading partials, i.e. $1/6[\bar{2}\,0\,2\,3] + 1/6[0\,\bar{2}\,2\,3] \rightarrow 1/3[\bar{1}\,\bar{1}\,2\,3]$.

In this second reaction, combination between partials produces a unit dislocation which of course involves an increase in energy, but in turn this unit dislocation can redissociate back to the original partials by cross-slip into an intersecting plane, which for this particular example consists of the $(1\,1\,\bar{2}\,2)$ plane, and would result in no net energy change. Other possible interactions between partials such as $1/6[\bar{2}\,0\,2\,3] + 1/6[2\,\bar{2}\,0\,3] = 1/3[0\,\bar{1}\,1\,3]$ generate false slip vectors for atom displacement and need not be considered. Before venturing an explanation of the dislocation array shown in Fig. 4, however, one further point is worthy of consideration, notably that stacking faults are essentially antiphase boundaries which involve the movement of large tungsten atoms

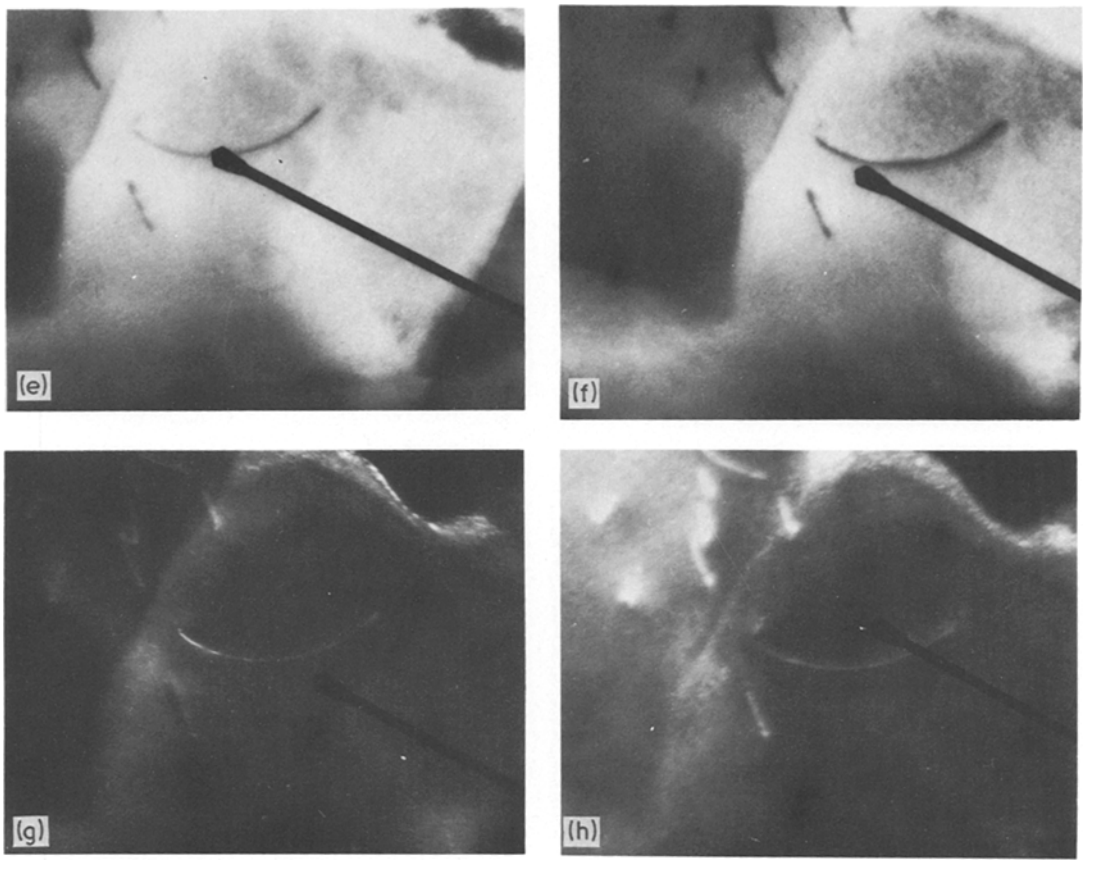

Figure 3 Continued.

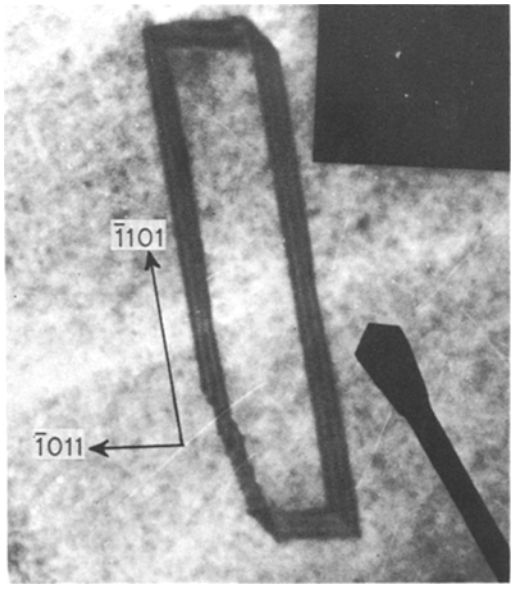

Figure 4 Extended dislocation network formed from a parallelogram of stacking faults. (Inset: $\{1\,0\,\bar{1}\,1\}$ diffraction pattern).

into the position of small carbon atoms and vice versa. This not only involves the breaking of extremely strong interatomic bonds, but also creates distortion due to atomic size misfit which will obviously add to the energy consideration when dislocation dissociation and interaction occurs. Strictly speaking, the energies associated with dislocation dissociation should also include an energy distortion term which is possibly responsible for the apparent ease of formation of dislocation networks when tungsten carbide is deformed. By adopting certain stable configurations within these networks it is possible that distortion stresses are counterbalanced by dislocations and the overall distortion minimized.

The dislocation structure observed in Fig. 4 can then be explained as interaction on intersecting planes to minimize dislocation strain energy and to reduce atomic misfit strains caused by antiphase regions created through partial dislocations. A suggested model for explaining these

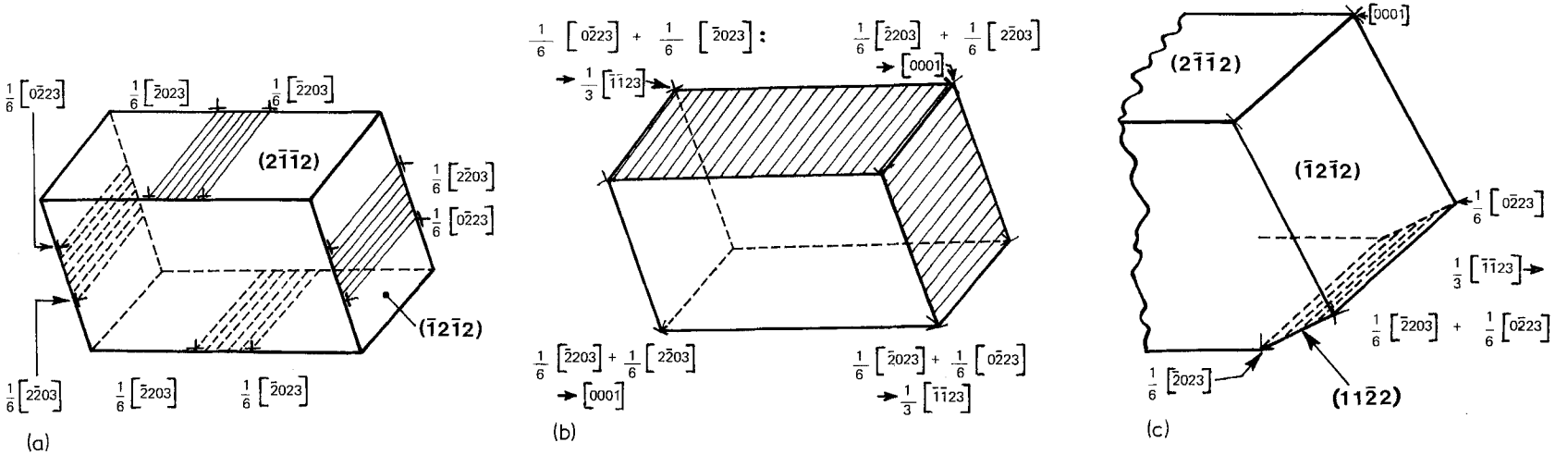

Figure 5 (a) Extended dislocations lying on intersecting $\{2\bar{1}\bar{1}2\}$ pyramidal planes before interaction. Note opposite sense partial dislocations on parallel planes to compensate for atomic misfit distortion. (b) Partial glide apart to react at intersection (c) $1/3[\bar{1}\bar{1}23]$ dislocation dissociates into partials and the $1/6[0\bar{2}23]$ partial cross-slip into the $(11\bar{2}2)$ plane.

occurrences which satisfies observed conditions is shown schematically in Fig. 5.

Effectively, the configuration produced reduces distortion stresses by placing tungsten and carbon atoms in counterbalancing positions on parallel slip planes, and further lowers the total dislocation strain energy by forming dislocations with [0 0 0 1] Burgers vectors from higher energy partials. The nodes at each corner of the parallelogram are effectively sessile since, at two corners, the resultant partials formed from $1/3\langle 1\,1\,\bar{2}\,3\rangle$ type dislocations can each slip into a plane specific to themselves and lock the node corner. Furthermore, although glissile [0 0 0 1] dislocations are formed at the other nodes of the network they too are bound by stacking faults and could not easily cross-slip into $\{1\,0\,\bar{1}\,0\}$ planes.

5. Conclusions

The centred dark-field technique appears to be somewhat less prone to error caused by factors which limit the effectiveness of other methods used to study dislocation in tungsten carbide, and has confirmed that slip can occur with $\langle 0\,0\,0\,1\rangle$ Burgers vectors operating on the $\{1\,0\,\bar{1}\,0\}$ slip planes.

Also shown, is direct visual evidence for dislocation dissociation, and analysis supports the model proposed by Johannesson and Lehtinen [7, 8] for dissociation reactions and partial interaction.

Finally, a model has been proposed for the locking of dislocations similar to that proposed by Lomer Cottrell in f c c metals, and is suggested as a reason responsible for the rigidity of dislocation networks formed by plastic deformation in tungsten carbide.

References

1. S. B. LUYCKX, *Acta. Met.* **16** (1968) 535.
2. B. O. JAENSSON, *Prakt. Met.* **9** (1972) 624.
3. *Idem, Mater. Sci. Eng.* **9** (1972) 339.
4. R. VENTER, S. CRITCHLEY and M. C. DeMALHERBE, *ibid.* **19** (1975) 201.
5. J. L. CHERMANT, *Powder Met.* **17** (1974) 85.
6. T. TAKAHASI and E. J. FREISE, *Phil. Mag.* **12** (1965) 1.
7. T. JOHANNESON and B. LEHTINEN, *Phys. Stat. Sol.* (1975) 615.
8. *Idem, Phil. Mag.* **18** (1971) 1079.

Received 6 March and accepted 22 May 1980.